Title

Hippo-TOR Signaling Crosstalks Underpin Microtubule Acetylation-linked Carcinogenesis in *Drosophila* Squamous Epithelia

Running title

Hippo-TOR signaling regulates microtubule acetylation

Authors

Rachita Bhattacharya[1, 2], Pradip Sinha[1, 2, *], and Nitin Mohan[1, 2, *]

[1]Biological Sciences and Bioengineering and [2]Mehta Family Center for Engineering in Medicine
Indian Institute of Technology Kanpur, India

[*]Corresponding authors
pradips@iitk.ac.in
nitinm@iitk.ac.in

ABSTRACT

Post-translational modifications (PTM), like acetylation, underpin the functional specialization of the cytoskeleton, such as microtubules (MT). For instance, acetylation of microbules is essential for cell flattening in *the Drosophila* adult squamous epithelia of female ovarian follicles and male accessory glands (MAG). Here we show that the highly conserved Hippo transcription co-factor Yorkie (Yki), a mechanosensor for cell flattening, regulates the acetylation of MT in squamous epithelia in both these organs. Yet, the fallouts of loss of nuclear Yki signaling are distinct in these two squamous epithelia. Thus, the knockdown of Yki in the squamous epithelia of ovarian follicles compromises their cell flattening. By contrast, knockdown of Yki in the MAG epithelium leads to its cancerous transformation which is suppressed by a simultaneous genetic ablation of MT-acetylation. We further note that Yki-knockdown-induced hyperacetylation of MT in MAG is TOR signaling-dependent. These results reveal that, while Yki-dependent acetylation of MT drives cell flattening, its cell type-specific homeostatic cross-talk with TOR signaling, as in the MAG, when dysregulated, culminates in carcinogenesis.

INTRODUCTION

Cell shape in eukaryotes is closely associated with their specialized functions (for review, see (Luxenburg and Zaidel-Bar, 2019)). During development, cell-signaling events tightly control morphological changes enabling cells to attain their final differentiated shape (for review, see (Albert Basson, 2012; Bernascone et al., 2017; Gillard and Röper, 2020)). Correspondingly, epithelial morphogenesis results in the development of terminally differentiated squamous, columnar, and cuboidal epithelia that line various organs and lumens, each serving diverse functions (Dasbiswas et al., 2018; Hannezo et al., 2014; Xiong et al., 2014). Squamous epithelial cells are much flatter than cuboidal precursors. These cell-shape remodelings are suggestive of mechanical forces invoked during development (Balaji et al., 2019) by targeting the cytoskeleton (Heisenberg and Bellaïche, 2013; Lecuit and Lenne, 2007; Singh et al., 2018). In particular, microtubule stability and dynamics are critical for distinct cellular architecture (for review, see (Matis, 2020)). The dynamic plus ends of the microtubules are projected to the cell boundary or they are tethered to the sites of adherens junction at the epithelial cell periphery (for review, see (Röper, 2020)). Thus microtubules can sense and respond to changes in cellular architecture by modulating their dynamics and organisation (for review, see (Röper, 2020)). Nonetheless, the mechanisms

regulating the mechanical properties of microtubules yielding to the cellular resilience required for epithelial morphogenesis remain poorly understood (for review, see (Matis, 2020)).

Tubulin post-translational modifications that render interphase cells with functionally distinct microtubule subsets play a pivotal role in differentially regulating microtubule stability and mechanics (for review, see (Janke and Magiera, 2020)). Among these modifications, alpha-tubulin K40 acetylation mediated by the highly conserved tubulin acetyltransferase (ATAT1), also known as MEC-17 in *Caenorhabditis elegans* (Neumann and Hilliard, 2014), is strongly associated with microtubule stability and enhanced microtubule mechanical flexibility (Portran et al., 2017; Xu et al., 2017). *In vitro*, acetylated tubulin is reported to be critical for cell polarity, intracellular transport, cell migration, and mechanosensation (Bance et al., 2019; Geiger et al., 2009; Seetharaman et al., 2022). Remarkably, in primary astrocytes cultured on substrates of varying stiffness, ATAT1 is shown to regulate focal adhesion turnover, promoting cell migration, and mechanosensitive cell adhesion (Seetharaman et al., 2022). Further, alveolar epithelial cells in culture exposed to mild cyclic stretch exhibit increased levels of acetylated microtubules, enabling cell stretching (Geiger et al., 2009). Moreover, loss of MEC-17 in zebrafish (Akella et al., 2010), mutant MEC-17 in *C. elegans* (Neumann and Hilliard, 2014), and ATAT1 depletion in mouse sensory neurons resulted in impaired touch and pain sensations (Morley et al., 2016), suggesting a conserved role of microtubule acetylation in mechanosensation.

In vivo, germline deletion of *Atat1* in mice, leading to complete loss of acetylated tubulin in tissues, however, showed viable, fertile mice with mildly distorted dentate gyrus and impaired sperm motility (Kim et al., 2013). Despite being dispensable for survival during development, microtubule acetylation is reported to be critical for cellular mechanics *in vivo*. For instance, *Atat1*$^{-/-}$ in mice showed defective neuronal migration leading to ventricular dilation due to hypoplasia in the septum and striatum (Li et al., 2019). In addition, α-tubulin acetylase (dTAT) is required for TRP channel NOMPC-mediated mechanosensation in *Drosophila* larvae (Yan et al., 2018). This mounting evidence suggests that microtubule acetylation is a key biochemical mechanism employed by cells in culture in response to external stimuli, as well as by cells within tissues in response to developmental cues, to modulate the mechanical properties of microtubules and provide protection from mechanical stress due to cell shape changes. However, except for a few *in vitro* studies where TGF-β-

activated kinase 1(TAK1) (Shah et al., 2018) and actin-MRTF-SRF is shown to regulate ATAT1 (Le Dour et al., 2022), our understanding of the molecular signaling that regulates microtubule acetylation *in vivo* remains limited, despite its importance for the cellular mechanical resilience during development.

Hippo signaling, beyond its central roles in organ size regulation, cell proliferation, and apoptosis, is a key critical in mediating cellular responses to mechanical cues such as changes in cell shape, extracellular matrix stiffness, and liquid shear forces. The cytoplasmic-to-nuclear translocation of the Hippo effectors and transcription cofactors Yki/YAP/TAZ is a hallmark of cell stretching and flattening. Interestingly, a recent report showed that a *Drosophila* microtubule-associated N-terminal acetyltransferase can modulate Hippo signaling for controlled organ growth (Mok and Choi, 2022). Additionally, in cultured fibroblasts, the knockdown of Atat1 abolished the association of the Hippo regulator Merlin with microtubules, thereby compromising the Hippo signaling-mediated control of cell proliferation (Aguilar et al., 2014). Taken together, these disparate pieces of evidence suggest that both microtubule acetylation and Hippo signaling are critical for integrating cellular responses to mechanical cues. Here, we investigate the role of Hippo signaling in regulating microtubule acetylation to achieve the cellular mechanical compliance required during epithelial morphogenesis and their deregulations in squamous cell carcinoma. Furthermore, our recent study demonstrated that, unlike its conventional role as a tumor promoter in organ-lining epithelium, nuclear Yorkie functions as a tumor suppressor in lumen-lining epithelial cells (Bhattacharya et al., 2023). Thus, it would be interesting to explore the effects of differential regulation of Hippo signaling on microtubule acetylation in the lumen versus the organ-lining epithelium during development.

RESULTS

Microtubule acetylation is critical for cell flattening in distinct squamous epithelia

In the *Drosophila* adult ovary, before stage 8, each egg chamber is composed of cuboidal epithelium (Wu et al., 2008). However, by stage 10, the egg chamber displays distinct anterior-posterior cell shape changes. The large nurse cells at the anterior of the chamber is covered by a thin squamous epithelium (SE), referred here as SE(N). In contrast, the columnar epithelium (CE), termed here as CE(O), lines the developing oocyte at the posterior (**Fig. 1A-C**). By stage 14, the nutrient contents of nurse cells are exhausted, and the SE(N)

enwrap and phagocytose the underlying nurse cells, eventually leading to SE (N) degeneration (Mondragon et al., 2019; Timmons et al., 2016). On the other hand, the posterior CE(O) stretches and progressively transitions from columnar to squamous to completely encapsulate the growing oocyte; these are designated as SE(O) (**Fig. 1A-C**) (for review, see (Duhart et al., 2017)). To assess the correlation between microtubule acetylation and cell flattening during epithelial morphogenesis, we immunostained wild-type follicles with acetylated-MT (**Fig. 1D-F**). Interestingly, we see elevated levels of acetylated-MT in the anterior squamous follicular epithelium SE(N), compared to the posterior columnar CE(O) at stage 10 (**Fig. 1D-E** and **H**). Furthermore, as the columnar epithelium stretches and transitions to squamous cells at stage 14, we observe a significant increase in MT-acetylation in the stretched squamous cells SE(O) compared to the columnar CE(O) (**Fig. 1E-F** and **H**). Here, the increase in cell area is quantified to assess the CE(O) to SE(O) transition (**Fig. 1G**).

As we see remarkable increase in MT-acetylation with cell stretching in the organ lining epithelium of follicle, we next validated our observation in the lumen lining epithelium of the paired adult male accessory gland (MAG), which is analogous to the mammalian prostate (Heifetz et al., 2000; Kumari and Sinha, 2021). The MAG is lined by a monolayer epithelium that has undergone tissue remodeling marked by a columnar-to-squamous cell shape transition (**Fig. 1I-K**, (Bhattacharya et al., 2023; Box et al., 2022)). Similar to the adult follicular counterpart, the MAG epithelium displays higher acetylated-MT levels during the transition from pupal columnar, CE(MAG) to adult squamous, SE(MAG) (**Fig. 1L-O**).

To confirm the significance of MT-acetylation in epithelial flattening, we knockdown the enzyme responsible for alpha-tubulin acetylation, *α-tat.* We generated somatic clones with *α-tat* knockdown (*hs-flp, act>α-tat-IR*) and immunostained for both acetylated and total tubulin. Indeed, we observed an absence of microtubule acetylation (MT-acet) in *α-tat* knockdown clones in comparison to wild-type neighbours, while the total tubulin levels remained unaltered (**Fig. S1**). A ubiquitous knockdown of *α-tat* driven by GR1-Gal4 (Goentoro et al., 2006) and ov-Gal4 (Herndon and Wolfner, 1995; Monsma et al., 1990) in follicular and MAG epithelia, respectively, downregulated the acetylation of microtubules with concomitant cell size reduction in stage 14 SE(O) follicles (**Fig. 1P-Q'** and **T**) and 7-day-old adult MAG SE (**Fig. 1R-S'** and **U**), indicative of compromised cell stretching with loss of acetylated-MT. Thus, a mere loss of MT-acetylation, despite no change in total

tubulin, can compromise cell size (**Fig. 1T-U**), suggesting the significance of MT-acetylation in epithelial flattening.

Altogether, a high level of MT-acetylation constitutes a columnar-to-squamous cell shape transition, and its loss abrogates cell flattening in both organ-lining follicles as well as lumen-lining MAG epithelia (**Fig. 1V**).

Loss of acetylated microtubules compromises membrane protein trafficking

Next, we investigated the functional role of the high levels of acetylated-MT observed during cell stretching. Previous studies have shown that cell-cell adhesion affects cell flattening. An exemplar being Fasciclin2 is an immunoglobulin family cell adhesion molecule that mediates homophilic cell adhesion between the lateral membranes of follicle cells (Szafranski and Goode, 2004). Tao, a serine/threonine kinase, promotes endocytosis of Fasciclin2, leading to its reduction in the lateral membrane during cuboidal-to-squamous cell shape transition (Gomez et al., 2012). In addition, a theoretical simulation also suggests that increased cell–cell lateral adhesion results in cell elongation or columnar cell formation, while reduction in adhesion can cause cell flattening (Hannezo et al., 2014). In line with these studies, Crumbs, an apical membrane protein (Tepass et al., 1990), has also been shown to apically dilute during columnar-to-squamous transition in response to mechanical strain experienced by the growing egg chamber (Fletcher et al., 2018) and male accessory gland (Bhattacharya et al., 2023) of *Drosophila.* Thus, membrane protein dilution via their enhanced endocytic trafficking is a critical mechanism that facilitates epithelial flattening *in vivo*.

Consistent with these reports, we noticed a dilution of the lateral membrane protein, FasIII (Wells et al., 2013), the sub-apical junction protein, Cadherin (Huang et al., 2012; Pope and Harris, 2008), and the basolateral protein, Lethal giant larva (Lgl) tumor suppressor (Aguilar-Aragon et al., 2020), with developmentally programmed squamous cell flattening (**Fig. S2)**.

Microtubules act as roadways for the intracellular transport of membrane proteins, such as Crumbs (Aguilar-Aragon et al., 2020) or adherens junction protein, like Cadherin (Harris and Peifer, 2007; Huang et al., 2012). Given that loss of microtubule acetylation compromised epithelial flattening in both SE(O) and SE(MAG) (see **Fig. 1P-U**), we asked if its loss affected endocytic trafficking of membrane proteins. Indeed, we see that loss of microtubule

acetylation sequesters FasIII (**Fig. 2A-A'**), Cad (**Fig. 2B-B'**) and Lgl (**Fig. 2C-C'**) at the cell boundaries of *α-tat-IR* clones, as confirmed by the increased intensity of the respective membrane proteins in the clone boundaries (**Fig. 2D-F**), in both follicle and MAG (**Fig. 2G-L**). Congruently, we also observed lodging of Rab5 marked early endosomes at the cell periphery (**Fig. 2M-N**). The enlarged Rab5 decorated vesicles lodged towards the periphery in the *α-tat-IR* clones, unlike the smaller Rab5 vesicles distributed throughout the cell is indicative of compromised endocytic cargo trafficking and processing (**Fig. 2M-N**). In addtion, we see the Rab5 vesicles lodged at the cell periphery co-localize with sequestered Lgl at the *α-tat-IR* clone boundaries (**Fig. 2O-P**). These observations suggest a functional role of microtubule acetylation in Rab5 mediated endocytic transport and dilution of Lgl (Papagiannouli, 2022) and other membrane proteins which likely precede cell flattening of the follicular SE (**Fig. 2Q**).

Microtubule acetylation regulates actin remodeling during epithelial flattening

Crosstalk between microtubules and the actin cytoskeleton is essential for maintaining cell shape, enabling cell migration, and facilitating intracellular transport (Tian et al., 2015) (for review, see (Dogterom and Koenderink, 2019)). Recent evidence suggests a dynamic interplay between microtubule acetylation and actin that facilitates *in vitro* cell stretching (Seetharaman et al., 2022). Therefore, we further investigated the effect of MT-acetylation on actin modulation in the epithelial flattening of follicle and MAG. Akin to actin depolymerisation in α-TAT1- depleted astrocytes in culture (Seetharaman et al., 2022), we observe significant actin severing and depolymerization, marked by phalloidin, in somatic clones with *α-tat* knockdown (*hs-flp, act>α-tat-IR*, **Fig. 3A-A''**) in squamous follicle epithelium, SE(O). Congruent to actin severing in *α-tat* knockdown clones, we also observe an upregulation of dephosphorylated cofilin (**Fig. 3B-B''**), which binds to and depolymerizes filamentous actin.

We next validated *α-tat* knockdown-mediated actin depolymerization in MAG squamous epithelia, SE(MAG). Unlike follicle epithelia, where we marked the actin filaments with phalloidin, here we used *a UAS-Life-Actin RFP* transgenic construct (Riedl et al., 2008), driven under SE(MAG)-specific *ovulin-Gal4* (Heifetz et al., 2000; Monsma et al., 1990). Since phalloidin robustly marks the muscle actin of MAG (Rambur et al., 2020), changes in epithelial actin upon *α-tat* knockdown were difficult to observe. Moreover, previous reports

have confirmed that Lifeact, a 17-amino-acid peptide, reliably marks filamentous actin (F-actin) structures in eukaryotic cells and tissues, and does not interfere with actin dynamics (Riedl et al., 2008). Our study using *UAS-Life-Actin RFP* in MAG (ov> *UAS-Life-Actin RFP*) reveal bundled actin in the squamous epithelia of control (**Fig. 3C**), which becomes sparse and depolymerized upon *α-tat* knockdown (*ov> UAS-Life-Actin RFP,α-tat-IR*, **Fig. 3D**). Thus, in addition to a defect in endocytic transport, loss of mt-acetylation dysregulates actin polymerization, thereby compromising epithelial flattening (**Fig. 3E**). Taken together, our results suggest a plausible role for microtubule acetylation in regulating actin polymerization and membrane protein dilution, where these well-coordinated events are critical for epithelial cell flattening during morphogenesis.

Yorkie differentially regulates microtubule acetylation in follicle and MAG squamous epithelia

Having identified the functional significance of elevated microtubule acetylation in epithelial cell flattening, we next examined the upstream molecular signaling that precisely tune the level of microtubule acetylation during epithelial morphogenesis. Molecular signaling pathways impinge upon cytoskeletal networks to exhibit their downstream effects and tune the spatio-temporal output and intensity of upstream signaling events (for review, see (Moujaber and Stochaj, 2020)). The Hippo pathway, one of the major signaling pathways responsive to the cellular mechanical cues, is regulated by cytoskeleton and cell junctional proteins (Dupont et al., 2011). Therefore, we investigated whether microtubule acetylation mediated by *α-tat* could regulate Hippo signaling.

The transcription co-factor of the Hippo pathway, YAP/TAZ/Yorkie, shows nuclear localization in response to epithelial cell stretching (Dupont et al., 2011; Moreno-Marmol et al., 2018) and mechanical strain (Fletcher et al., 2018; Friesen and Hariharan, 2023).To test whether MT-acetylation is required for Yorkie nuclear translocation during epithelial flattening of SE(O) and SE(MAG), we first knocked down *α-tat* in squamous epithelia of follicle, SE(O), and investigated Yorkie localization using Yki-GFP reporter construct. We observe nuclear Yki-GFP in *α-tat* knockdown somatic clones (RFP-negative), comparable to its wild-type neighbours (**Fig. 4A-A'**). Likewise, loss of microtubule acetylation via *α-tat* knockdown in MAG, also display nuclear Yki localization and signaling, comparable to

control (**Fig. 4B-B', Fig. S3**). Our results therefore reveal that MT-acetylation is not required for nuclear translocation of Yorkie during epithelial flattening. Together with our previous observation that MT-acetylation increases with cell stretching, we now speculate that MT-acetylation is downstream of the nuclear Yki signaling. To test this, we knockdown *yki* in follicle SE(O) and SE (MAG) and compared level of acetylated-MT with respective controls. Interestingly, we observe loss of acetylated-MT with knockdown of *yki* in the squamous follicle epithelium (**Fig. 4D-E**), as opposed to elevated levels of acetylated-MT upon knockdown of *yki* in adult MAG squamous epithelium (**Fig. 4F-G**). We wonder if such differential regulation of MT-acetylation by Yki in MAG and follicle could determine the disparate functional outcomes of Yki gain or loss in these two tissues.

While nuclear translocation of YAP/TAZ/Yki is physiologically essential for squamous epithelial morphogenesis in response to organ growth (Fletcher et al., 2018; Friesen and Hariharan, 2023; Mahoney et al., 2014; Moreno-Marmol et al., 2018), its aberrant gain or loss has been implicated in squamous cell carcinoma (SCC) (for review, see (Fu et al., 2022; Luo et al., 2023)). While loss of Yki in SE of ovarian follicle results in cell size reduction (**Fig. S3**, (Fletcher et al., 2018; Friesen and Hariharan, 2023)), with no oncogenic fallout, Yki knockdown in MAG results in cellular hypertrophy (**Fig. S3**), leading to MAG-SCC (Bhattacharya et al., 2023). Our recent study addressed the disparity in Yki function in distinct tissues and revealed that Yki is a tumor suppressor in lumen lining SE, similar to the MAG epithelium, as opposed to the conventional role of Yki as tumor promotor in organ lining SE, like the follicle. Therefore, the downstream effector by which Yki regulates MT-acetylation could be different during epithelial cell stretching in the follicle versus MAG.

YAP/TAZ/Yki modulation in epithelial cells mediates its effect via PI3K/Akt/TOR signaling (for review, see (Honda et al., 2023)). Recently, we have shown a paradoxical association between Yki and TOR signaling in SEs of MAG, such that, Yki negatively regulates TOR (Bhattacharya et al., 2024), as opposed to its positive correlation with TOR in other epithelial tissues (Tumaneng et al., 2012). Whether activated PI3K/Akt/TOR signaling regulates microtubule acetylation, is not known. Thus, we modulated Akt signaling in the SEs of both MAG and follicle and observed its effect on microtubule acetylation. We observe that Akt upregulation (*ov>myr-Akt*) increases MT-acet, while Akt knockdown (*ov>Akt-IR*) decreases MT-acet, in both follicle (**Fig. 4H-I**) and MAG SEs (**Fig. 4J-K**). Thus, Akt signaling positively co-relates with MT-acetylation levels in both squamous epithelia. However,

knockdown of *α-tat* in squamous follicle epithelia (*c204>α-tat*-IR) upregulates the TOR target, pS6K (**Fig. 4L-N**), contrary to the downregulation of pS6K with knockdown of *α-tat* in MAG squamous cells (**Fig. 4O-Q**). These results suggest that MT-acetylation mediated by α-tat differentially regulates TOR activity in MAG and follicle SE, such that, α-tat positively regulates TOR signaling in MAG, but inhibits it in follicle SE.

Overall, our results delineate the differential mechanisms by which Yki regulates MT-acetylation in follicle versus MAG. In follicle, Yki positively regulates PI3K/Akt/TOR, which in turn positively regulates MT-acetylation. Therefore, loss of Yki results in the loss of acetylated microtubules in the follicle. By contrast, in MAG, Yki negatively regulates PI3K/Akt/TOR (Bhattacharya et al., 2023), which in turn positively regulates MT-acetylation. Therefore, loss of Yki results in the upregulation of PI3K/Akt/TOR (Bhattacharya et al., 2023), thereby increasing microtubule acetylation and prefiguring SCC in the MAG (Bhattacharya et al., 2023).

Loss of microtubule acetylation rescues Yki loss driven SCC in MAG

Hyperacetylation of microtubules has also been established as a prognostic biomarker in most carcinoma, including SCC (for review, see (Nekooki-Machida and Hagiwara, 2020)). Indeed, MT-hyperacetylation, upon knockdown of *HDAC6*, a tubulin deacetylating enzyme (Łysyganicz et al., 2021), is sufficient to increase organ size in MAG (**Fig. 5A-C**), eventually resulting in a complete cytoarchitectural disruption (**Fig. 5D-D'**), reminiscent of MAG-SCC (Bhattacharya et al., 2023). Previously, we have shown that MAG-SCC entails Yki loss and upregulation of TOR activity (Bhattacharya et al., 2023). Thus, we asked whether HDAC6 knockdown impinges upon downregulated Yki signaling and TOR hyperactivity. Interestingly, upon *HDAC6* knockdown in adult MAG, we observe the nuclear expression of Diap1-lacZ (**Fig. 5E-E'**), which was comparable to that of the control (**Fig. S3**), suggesting unaltered nuclear Yki signaling. However, we observe an upregulation of the TOR target, pS6K (**Fig. 5F-H**), thereby explaining HDAC6 knockdown-induced organ size increase and cytoarchitectural disruption in MAG.

We next validated whether microtubules become hyperacetylated in our SCC model. We observe MT-hyperacetylation upon Yki gain (but not Yki loss (see Fig. 4D-E)) in follicle SE

(**Fig. S4**). By contrast the adult MAG displayed yki-loss dependent MT-hyperacetylation during MAG-SCC (**Fig. 5I-J''**). A concomitant increase in MT-acetylation also correlates with increased cell size and disruption of the cytoarchitecture (**Fig. S4,** (Bhattacharya et al., 2023)).

Given that loss of MT-acetylation decreases TOR activity in MAG (see, **Fig. 4O-Q**), we speculate downregulating microtubule acetylation could rescue MAG-SCC induced by Yki loss (Bhattacharya et al., 2023). Indeed, we observe that *α-tat* knockdown reduced MT-acetylation in adult MAG bearing Yki loss (**Fig. 5K-K''**). We also observe restoration of cell size and architecture in MAG SE with simultaneous knockdown of *yki* and *α-tat* (**Fig. 5L-O**), along with improved lifespan of adults (**Fig. 5P**).

Our results therefore highlight the pro-tumorigenic effect of MT-acetylation in Yorkie loss-induced MAG-SCC.

DISCUSSION

One of the enduring challenges in cancer biology is the cell-type specificity of oncogenic lesions (for review, see (Bianchi et al., 2020; Peters et al., 2024; Schneider et al., 2017; Sieber et al., 2005). The question of why an oncogenic lesion in one cell type fails to transform another with comparable cellular attributes presents the challenge of resolution in a case by case manner. Here we have addressed this paradox in the squamous epithelia of two *Drosophila* adult organs: ovarian follicles and MAG. While both display mechanical strain-linked nuclear Yki signaling, its knockdown induces SCC in the MAG, but not in their ovarian follicular counterparts. Here we show that these contrasting outcomes stem from the impact of the knockdown of Yki signaling on a post-translational modification, namely, acetylation of microtubules in cell-type-specific manner. In MAG, loss of Yki signaling induces hyperacetylation of the microtubules, a well-known cancer-promoting cytoskeletal perturbation (Boggs et al., 2015; Chakrabarti et al., 2015; Saba et al., 2014). By contrast, the knockdown of Yki signaling in the ovarian follicular epithelium induces loss of microtubule acetylation, a condition that has been previously shown to impede tumor progression (Chien et al., 2016).

We further reveal that this disparate regulation of microtubule acetylation likely stems from the peculiarities of squamous cell type-specificities of Hippo-TOR crosstalk. While both ovarian follicular and MAG squamous epithelia display nuclear Yki (Bhattacharya et al., 2023; Fletcher et al., 2018; Friesen and Hariharan, 2023), indicating perpetual Hippo signaling, its crosstalk with the cell growth-sensing TOR signaling is disparate. In MAG, nuclear Yki signaling coincides with their cell flattening and attainment of programmed adult cell sizes (Bhattacharya et al., 2023). Unsurprisingly, Yki signaling in MAG suppresses the growth sensing TOR signaling, which when reversed induces SCC (Bhattacharya et al., 2023). During columnar-to-squamous transition of follicle epithelium (stage 9-stage 14), too, Yki displays nuclear localization from stage 11 onwards (coinciding with cell flattening). However, in these flattening follicular epithelium TOR signaling appears permissive (Borreguero-Muñoz et al., 2019; Halder et al., 2022): that is, not subjected to suppression unlike their MAG counterparts. This subtle differences in Hippo-TOR signaling crosstalk in these two organs likely underpin distinct fallouts of Yki signaling loss. Thus, a Yki-loss-induced gain of TOR signaling leads to increased acetylation of microtubules, culminating in MAG-SCC, while in the follicle counterparts, the loss of Yki signaling downregulates TOR signaling (and consequently, acetylation of microtubules).

Tubulin hyperacetylation influences cancer behaviors, such as intracellular trafficking (Gao et al., 2010). For example, a deficiency in HDAC6 can increase tubulin acetylation, promoting the microtubule-directed transport of epidermal growth factor receptor (EGFR)-loaded vesicles in lung cancer (Gao et al., 2010). The loss of intercellular junctions in MAG SCC likely correlates with elevated endocytic trafficking of membrane proteins on hyperacetylated microtubules. In this scenario, the loss of intercellular junctions was arrested by knocking down *α–tat* and, consequently, a rescue of MAG SCC. Microtubules are one of the primary targets for anticancer drugs because of their role in cell proliferation and migration (for review, see (Jordan and Wilson, 2004)). However, as anticancer drugs targeting MT display side effects, including the death of normal cells, it is imperative to develop anticancer agents targeting a subset of MTs, such as acetylated-MTs, of only cancer cells. Our study identifying the similarities and distinctions in the regulation of MT-acetylation in disparate tissues would help to develop therapeutic strategies targeting MT-acetylation for cancer with more specificities.

MATERIALS AND METHODS

Drosophila maintenance and generation of somatic clones

The fly lines were maintained at 25°C on standard yeast corn-meal agar food unless otherwise stated. The genetic knockdown and overexpression experiments in MAG and follicles were done at 29°C to increase the efficiency of Gal4 activity (Duffy, 2002). The ov-Gal4 experiments were performed as described in our previous study (Bhattacharya et al., 2023). For experiments involving GR1-Gal4 and c204-Gal4, the eclosed female flies were shifted to 29°C and fattened with yeast-paste supplement for 4-5 days until dissection. Induction of transgenes using flp/FRT-flip-out Gal4, was performed by crossing flies of genotype *hs-flp, act>CD2>Gal4 UAS-GFP* or *hs-flp UAS-mCD8:GFP, act>CD2>Gal4* (Sahu et al., 2021) with the desired UAS transgenes. The F1 adult flies with appropriate genotypes were given heat shock at 37°C. For crosses with *hs-flp, act>CD2>Gal4 UAS-GFP*, heat shock was given for 5 min to 5-day-old adult males, while 10-20 min to 5-day-old adult females. For crosses with *hs-flp UAS-mCD8:GFP, act>CD2>Gal4* (Fig. S4), the F1 female progeny were subjected to heat shock for 1 hour duration thrice a day for three consecutive days (Sahu et al., 2021). After heat shock, the adult female flies were fattened at 29°C for 5 days and then dissected, while the adult males were dissected on 10 and 20 days for the assessment of *α-tat* and *HDAC6* knockdown clones, respectively. The details of the fly strains, reagents, and resources are provided in the Key Resource Table.

Immunostaining and microscopy

MAG and ovarian follicles were dissected in cold PBS and fixed in 4% paraformaldehyde. Tissues were permeabilised in PBST (1XPBS containing 0.02% Triton-X-100). After blocking in 5% BSA for 2 h, they were incubated with primary antibody overnight at 4°C, washed three times for 10 min each in PBST, and then incubated with appropriate fluorescent-tagged secondary antibodies (1:250, Invitrogen) for two hours at room temperature. The samples were washed three times for 10 min each in PBST, followed by two washes for 10 min each in PBS, and counterstained with TO-PRO-3 and/or Alexa Fluor™ 555 phalloidin (A34055, Invitrogen), wherever appropriate. Finally, the tissues were washed thrice for 10 min each in PBS, mounted in Vectashield®, and sealed with nail paint.

The samples were imaged with a 20X air, 40X oil, or 63X oil immersion objective using a Leica SP5 laser scanning confocal microscope. All images were assembled using the Adobe Illustrator.

Quantification and statistical analysis

The cell area and fluorescence intensity were calculated using FIJI. A freehand drawing tool was used to trace the cell or organ boundaries and calculate the surface area and integrated density. All image acquisitions, particularly those involving fluorescence intensity measurements, were performed using the same parameters for control and test samples. To quantify the fluorescence intensity of acetylated tubulin in the columnar and squamous follicle areas, the integrated density in each case was normalised to their respective average cell area. For other experiments, the fluorescence integrated density from the desired protein of interest was normalised to the maximum intensity across all genotypes. Colocalisation analysis was performed using the Coloc2 plugin in FIJI.

All statistical analyses were performed using GraphPad 9.0. Unpaired *t*-test were performed to quantify cell, organ, and nuclear sizes. A cutoff of $p>0.05$ was used to define statistical significance in all graphical plots. Illustrations were made using the Adobe Illustrator.

Key Resource Table

REAGENTS OR RESOURCE	SOURCE	IDENTIFIER
Antibodies		
Mouse anti-FasIII	DSHB	7G10
Mouse anti-α-tubulin	DSHB	12G10
Mouse anti-β-Gal	Sigma-Aldrich	G6282
	DSHB	40-1a
Rabbit anti-Lgl	Sigma-Aldrich	Gift from Fumio Matsuzaki
Rat anti-DE-cadherin	DSHB	DCAD2

Rabbit anti-S6K	CST	9205
Rabbit anti p-4EBP	CST	2855
Rabbit anti-α-tubulin	Abcam	ab18251
Mouse anti-acetylated tubulin	Sigma-Aldrich	T6793
Guinea pig anti-Rab5	NA	Gift from Akira Nakamura
Alexa Fluor 488 Goat anti-mouse IgG	Invitrogen	A11007
Alexa Fluor 555 Goat anti-mouse IgG	Invitrogen	A32727
Alexa Fluor 633 Goat anti-mouse IgG	Invitrogen	A21050
Alexa Fluor 488 Goat anti-rabbit IgG	Invitrogen	A21206
Alexa Fluor 555 Goat anti-rabbit IgG	Invitrogen	A21428
Alexa Fluor 633 Goat anti-rabbit IgG	Invitrogen	A21070
TO-PRO-3	Invitrogen	S33025
Phalloidin-555	Invitrogen	A34055
Vectashield	Vector Laboratories	#H-1000
Software and Algorithms		
Leica LAS AF software	Leica microsystem	http://www.leicamicrosystems.com/productes/microscope-software/
Prism	Graph pad	https://www.graphpad.com/
Illustrator	Adobe CC	http://www.adobe.com
FIJI	ImageJ	https://imagej.net/software/fiji/
Other		
Leica TCS SP5 microscope	Leica microsystem	
***Drosophila* strains**		

UAS-GFP.nls	BDSC	RRID: BDSC_4776
UAS-yki-RNAi	BDSC	RRID: BDSC_34067
Diap1-lacZ	BDSC	RRID:BDSC_12093
UAS-myr-Akt	BDSC	RRID:BDSC_80935
UAS-Akt-RNAi	BDSC	RRID:BDSC_82957
UAS-yki^{3SA}	BDSC	RRID:BDSC_28817
UAS-yki^{S168A}	BDSC	RRID:BDSC_28816
FasIII:GFP	BDSC	RRID:BDSC_59809
UAS-α-tat-RNAi	BDSC	RRID:BDSC_62331
UAS-α-tat-RNAi	BDSC	RRID:BDSC_28777
UAS-HDAC6-RNAi	BDSC	RRID:BDSC_31053
UAS-Lifeact-RFP	BDSC	RRID:BDSC_58362
GR1-Gal4	BDSC	RRID:BDSC_36287
C204-Gal4	BDSC	RRID:BDSC_3751
hs-flp, act>CD2>Gal4, UAS GFP	Lab generated	
hs-flp UAS-mCD8:GFP, act>CD2>Gal4	Gift form Mohit Prasad	
Yki-GFP	Gift from Barry Thompson	
ovulin-Gal4	Gift from Kristipati Ravi Ram	

FUNDING

This study was supported by research grants from the Science and Engineering Research Board (SERB) to NM (Project No. SERB/F/3894/2023-2024) and the Department of Science

and Technology (DST) Ministry of Science and Technology India to PS (Project No. EMR/2016/006723). We would like to thank the Indian Council of Medical Research (ICMR) for financial support to RB.

AUTHOR CONTRIBUTIONS

RB and NM conceived and planned all investigations. RB conducted all experiments. NM supervised the study. RB, PS and NM wrote the manuscript.

CONFLICT OF INTEREST

The authors declare that they have no conflict of interest.

ACKNOWLEDGEMENTS

We thank Barry Thompson, Kristipati Ravi Ram, and Mohit Prasad for fly stocks, and Jonaki Sen for the cofilin antibody.

REFERENCES

Aguilar-Aragon, M., Fletcher, G. and Thompson, B. J. (2020). The cytoskeletal motor proteins Dynein and MyoV direct apical transport of Crumbs. *Dev. Biol.* **459**, 126–137.

Aguilar, A., Becker, L., Tedeschi, T., Heller, S., Iomini, C. and Nachury, M. V. (2014). α-tubulin K40 acetylation is required for contact inhibition of proliferation and cell-substrate adhesion. *Mol. Biol. Cell* **25**, 1854–1866.

Akella, J. S., Wloga, D., Kim, J., Starostina, N. G., Lyons-Abbott, S., Morrissette, N. S., Dougan, S. T., Kipreos, E. T. and Gaertig, J. (2010). MEC-17 is an α-tubulin acetyltransferase. *Nature* **467**, 218–222.

Albert Basson, M. (2012). Signaling in cell differentiation and morphogenesis. *Cold Spring Harb. Perspect. Biol.* **4**, 1–21.

Balaji, R., Weichselberger, V. and Classen, A.-K. (2019). Response of Drosophila epithelial cell and tissue shape to external forces in vivo. *Development* **146**, dev171256.

Bance, B., Seetharaman, S., Leduc, C., Boeda, B. and Etienne-Manneville, S. (2019). Microtubule acetylation but not detyrosination promotes focal adhesion dynamics and astrocyte migration. *J. Cell Sci.* **132**, jcs225805.

Bernascone, I., Hachimi, M. and Martin-Belmonte, F. (2017). Signaling networks in epithelial tube formation. *Cold Spring Harb. Perspect. Biol.* **9**, 1–20.

Bhattacharya, R., Kumari, J., Banerjee, S., Tripathi, J., Mohan, N. and Sinha, P. (2023). Hippo effector, Yorkie, is a tumor suppressor in select Drosophila squamous epithelia. *bioRxiv*.

Bianchi, J. J., Zhao, X., Mays, J. C. and Davoli, T. (2020). Not all cancers are created equal: Tissue specificity in cancer genes and pathways. *Curr. Opin. Cell Biol.* **63**, 135–143.

Boggs, A. E., Vitolo, M. I., Whipple, R. A., Charpentier, M. S., Goloubeva, O. G., Ioffe, O. B., Tuttle, K. C., Slovic, J., Lu, Y., Mills, G. B., et al. (2015). α-Tubulin acetylation elevated in metastatic and basal-like breast cancer cells promotes microtentacle formation, adhesion, and invasive migration. *Cancer Res.* **75**, 203–215.

Borreguero-Muñoz, N., Fletcher, G. C., Aguilar-Aragon, M., Elbediwy, A., Vincent-Mistiaen, Z. I. and Thompson, B. J. (2019). The Hippo pathway integrates PI3K–Akt signals with mechanical and polarity cues to control tissue growth. *PLoS Biol* **17**, e3000509.

Box, A. M., Church, S. J., Nandakumar, S., Prasad, D., Afrakhteh, A., Taichman, R. S. and Buttitta, L. (2022). Endocycles support tissue growth and regeneration of the adult Drosophila accessory gland. *bioRxiv*.

Chakrabarti, K. R., Whipple, R. A., Boggs, A. E., Hessler, L. K., Bhandary, L., Vitolo, M. I., Thompson, K. and Martin, S. S. (2015). Pharmacologic regulation of AMPK in breast cancer affects cytoskeletal properties involved with microtentacle formation and re-attachment. *Oncotarget* **6**, 36292–36307.

Chien, J. Y., Tsen, S. D., Chien, C. C., Liu, H. W., Tung, C. Y. and Lin, C. H. (2016). αTAT1 downregulation induces mitotic catastrophe in HeLa and A549 cells. *Cell Death Discov.* **2**, 1–9.

Dasbiswas, K., Hannezo, E. and Gov, N. S. (2018). Theory of epithelial cell shape transitions induced by mechanoactive chemical gradients. *Biophys. J.* **114**, 968–977.

Dogterom, M. and Koenderink, G. H. (2019). Actin–microtubule crosstalk in cell biology. *Nat. Rev. Mol. Cell Biol.* **20**, 38–54.

Duffy, J. B. (2002). GAL4 system in Drosophila: A fly geneticist's Swiss army knife. *Genesis* **34**, 1–15.

Duhart, J. C., Parsons, T. T. and Raftery, L. A. (2017). The repertoire of epithelial morphogenesis on display: Progressive elaboration of Drosophila egg structure. *Mech.*

Dev. **148**, 18–39.

Dupont, S., Morsut, L., Aragona, M., Enzo, E., Giulitti, S., Cordenonsi, M., Zanconato, F., Le Digabel, J., Forcato, M., Bicciato, S., et al. (2011). Role of YAP/TAZ in mechanotransduction. *Nature* **474**, 179–184.

Fletcher, G. C., Diaz-de-la-Loza, M.-D.-C., Borreguero-Muñoz, N., Holder, M., Aguilar-Aragon, M. and Thompson, B. J. (2018). Mechanical strain regulates the Hippo pathway in Drosophila. *Development* **145**, dev159467.

Friesen, S. and Hariharan, I. K. (2023). Coordinated growth of linked epithelia is mediated by the Hippo pathway. *bioRxiv*.

Fu, M., Hu, Y., Lan, T., Guan, K.-L., Luo, T. and Luo, M. (2022). The Hippo signalling pathway and its implications in human health and diseases. *Signal Transduct. Target. Ther.* **7**, 1–20.

Gao, Y. S., Hubbert, C. C. and Yao, T. P. (2010). The microtubule-associated histone deacetylase 6 (HDAC6) regulates epidermal growth factor receptor (EGFR) endocytic trafficking and degradation. *J. Biol. Chem.* **285**, 11219–11226.

Geiger, R. C., Kaufman, C. D., Lam, A. P., Budinger, G. R. S. and Dean, D. A. (2009). Tubulin acetylation and histone deacetylase 6 activity in the lung under cyclic load. *Am. J. Respir. Cell Mol. Biol.* **40**, 76–82.

Gillard, G. and Röper, K. (2020). Control of cell shape during epithelial morphogenesis: recent advances. *Curr. Opin. Genet. Dev.* **63**, 1–8.

Goentoro, L. A., Yakoby, N., Goodhouse, J., Schüpbach, T. and Shvartsman, S. Y. (2006). Quantitative analysis of the GAL4/UAS system in Drosophila oogenesis. *Genesis* **44**, 66–74.

Gomez, J. M., Wang, Y. and Riechmann, V. (2012). Tao controls epithelial morphogenesis by promoting Fasciclin 2 endocytosis. *J. Cell Biol.* **199**, 1131–43.

Halder, S., Ghosh, G., Gayen, B. and Prasad, M. (2022). TOR signalling regulates epithelial cell shape transition in Drosophila oogenesis. *bioRxiv*.

Hannezo, E., Prost, J. and Joanny, J.-F. (2014). Theory of epithelial sheet morphology in three dimensions. *Proc. Natl. Acad. Sci.* **111**, 27–32.

Harris, T. J. C. and Peifer, M. (2007). aPKC controls microtubule organization to balance adherens junction symmetry and planar polarity during development. *Dev. Cell* **12**, 727–738.

Heifetz, Y., Lung, O., Frongillo, E. A. and Wolfner, M. F. (2000). The Drosophila seminal fluid protein Acp26Aa stimulates release of oocytes by the ovary. *Curr. Biol.* **10**, 99–

102.

Heisenberg, C. P. and Bellaïche, Y. (2013). Forces in tissue morphogenesis and patterning. *Cell* **153**, 948.

Herndon, L. A. and Wolfner, M. F. (1995). A Drosophila seminal fluid protein, Acp26Aa, stimulates egg laying in females for 1 day after mating. *Proc. Natl. Acad. Sci.* **92**, 10114–10118.

Honda, D., Okumura, M. and Chihara, T. (2023). Crosstalk between the mTOR and Hippo pathways. *Dev. Growth Differ.* **65**, 337–347.

Huang, J., Huang, L., Chen, Y. J., Austin, E., Devor, C. E., Roegiers, F. and Hong, Y. (2012). Differential regulation of adherens junction dynamics during apical-basal polarization. *Development* **139**, 4001–4013.

Janke, C. and Magiera, M. M. (2020). The tubulin code and its role in controlling microtubule properties and functions. *Nat. Rev. Mol. Cell Biol.* **21**, 307–326.

Jordan, M. A. and Wilson, L. (2004). Microtubules as a target for anticancer drugs. *Nat. Rev. Cancer* **4**, 253–265.

Kim, G. W., Li, L., Gorbani, M., You, L. and Yang, X. J. (2013). Mice lacking α-tubulin acetyltransferase 1 are viable but display α-tubulin acetylation deficiency and dentate gyrus distortion. *J. Biol. Chem.* **288**, 20334–20350.

Kumari, J. and Sinha, P. (2021). Developmental expression patterns of toolkit genes in male accessory gland of Drosophila parallels those of mammalian prostate. *Biol. Open* **10**, bio058722.

Le Dour, C., Chatzifrangkeskou, M., Macquart, C., Magiera, M. M., Peccate, C., Jouve, C., Virtanen, L., Heliö, T., Aalto-Setälä, K., Crasto, S., et al. (2022). Actin-microtubule cytoskeletal interplay mediated by MRTF-A/SRF signaling promotes dilated cardiomyopathy caused by LMNA mutations. *Nat. Commun.* **13**, 7886.

Lecuit, T. and Lenne, P.-F. (2007). Cell surface mechanics and the control of cell shape, tissue patterns and morphogenesis. *Nat. Rev. Mol. Cell Biol.* **8**, 633–644.

Li, L., Jayabal, S., Ghorbani, M., Legault, L. M., McGraw, S., Watt, A. J. and Yang, X. J. (2019). ATAT1 regulates forebrain development and stress-induced tubulin hyperacetylation. *Cell. Mol. Life Sci.* **76**, 3621–3640.

Luo, J., Deng, L., Zou, H., Guo, Y., Tong, T., Huang, M., Ling, G. and Li, P. (2023). New insights into the ambivalent role of YAP/TAZ in human cancers. *J. Exp. Clin. Cancer Res.* **42**, 1–22.

Luxenburg, C. and Zaidel-Bar, R. (2019). From cell shape to cell fate via the cytoskeleton

— Insights from the epidermis. *Exp. Cell Res.* **378**, 232–237.

Łysyganicz, P. K., Pooranachandran, N., Liu, X., Adamson, K. I., Zielonka, K., Elworthy, S., van Eeden, F. J., Grierson, A. J. and Malicki, J. J. (2021). Loss of deacetylation enzymes Hdac6 and Sirt2 promotes acetylation of cytoplasmic tubulin, but suppresses axonemal acetylation in zebrafish cilia. *Front. Cell Dev. Biol.* **9**, 1–14.

Mahoney, J. E., Mori, M., Szymaniak, A. D., Varelas, X. and Cardoso, W. V. (2014). The Hippo pathway effector Yap controls patterning and differentiation of airway epithelial progenitors. *Dev. Cell* **30**, 137–150.

Matis, M. (2020). The mechanical role of microtubules in tissue remodeling. *BioEssays* **42**, 1–7.

Mok, J. W. and Choi, K. W. (2022). Modulation of Hippo signaling by Mnat9 N-acetyltransferase for normal growth and tumorigenesis in Drosophila. *Cell Death Dis.* **13**, 1–7.

Mondragon, A. A., Yalonetskaya, A., Ortega, A. J., Zhang, Y., Naranjo, O., Elguero, J., Chung, W. S. and McCall, K. (2019). Lysosomal machinery drives extracellular acidification to direct non-apoptotic cell death. *Cell Rep.* **27**, 11–19.

Monsma, S. A., Harada, H. A. and Wolfner, M. F. (1990). Synthesis of two Drosophila male accessory gland proteins and their fate after transfer to the female during mating. *Dev. Biol.* **142**, 465–475.

Moreno-Marmol, T., Cavodeassi, F. and Bovolenta, P. (2018). Setting eyes on the retinal pigment epithelium. *Front. Cell Dev. Biol.* **6**, 145.

Morley, S. J., Qi, Y., Iovino, L., Andolfi, L., Guo, D., Kalebic, N., Castaldi, L., Tischer, C., Portulano, C., Bolasco, G., et al. (2016). Acetylated tubulin is essential for touch sensation in mice. *Elife* **5**, 25.

Moujaber, O. and Stochaj, U. (2020). The cytoskeleton as regulator of cell signaling pathways. *Trends Biochem. Sci.* **45**, 96–107.

Nekooki-Machida, Y. and Hagiwara, H. (2020). Role of tubulin acetylation in cellular functions and diseases. *Med. Mol. Morphol.* **53**, 191–197.

Neumann, B. and Hilliard, M. A. (2014). Loss of MEC-17 leads to microtubule instability and axonal degeneration. *Cell Rep.* **6**, 93–103.

Papagiannouli, F. (2022). Endocytosis at the crossroad of polarity and signaling regulation: Learning from Drosophila melanogaster and beyond. *Int. J. Mol. Sci.* **23**, 4684.

Peters, L., Venkatachalam, A. and Ben-Neriah, Y. (2024). Tissue-predisposition to cancer driver mutations. *Cells* **13**, 1–15.

Pope, K. L. and Harris, T. J. C. (2008). Control of cell flattening and junctional remodelling during squamous epithelial morphogenesis in Drosophila. *Development* **135**, 2227–2238.

Portran, D., Schaedel, L., Xu, Z., Théry, M. and Nachury, M. V (2017). Tubulin acetylation protects long-lived microtubules against mechanical ageing.

Rambur, A., Lours-Calet, C., Beaudoin, C., Buñay, J., Vialat, M., Mirouse, V., Trousson, A., Renaud, Y., Lobaccaro, J.-M. A., Baron, S., et al. (2020). Sequential Ras/MAPK and PI3K/AKT/mTOR pathways recruitment drives basal extrusion in the prostate-like gland of Drosophila. *Nat. Commun.* **11**, 2300.

Riedl, J., Crevenna, A. H., Kessenbrock, K., Yu, J. H., Neukirchen, D., Bista, M., Bradke, F., Jenne, D., Holak, T. A., Werb, Z., et al. (2008). Lifeact: A versatile marker to visualize F-actin. *Nat. Methods* **5**, 605–607.

Röper, K. (2020). Microtubules enter centre stage for morphogenesis. *Philos. Trans. R. Soc. B Biol. Sci.* **375**,.

Saba, N. F., Magliocca, K. R., Kim, S., Muller, S., Chen, Z., Owonikoko, T. K., Sarlis, N. J., Eggers, C., Phelan, V., Grist, W. J., et al. (2014). Acetylated tubulin (AT) as a prognostic marker in squamous cell carcinoma of the head and neck. *Head Neck Pathol.* **8**, 66–72.

Sahu, A., Karmakar, S., Halder, S., Ghosh, G., Acharjee, S., Dasgupta, P., Ghosh, R., Deshpande, G. and Prasad, M. (2021). Germline soma communication mediated by gap junction proteins regulates epithelial morphogenesis. *PLoS Genet.* **17**, 1–32.

Schneider, G., Schmidt-supprian, M., Rad, R. and Saur, D. (2017). Tissue-specific tumorigenesis: context matters. *Nat. Rev. Cancer* **17**, 239.

Seetharaman, S., Vianay, B., Roca, V., Farrugia, A. J., De Pascalis, C., Boëda, B., Dingli, F., Loew, D., Vassilopoulos, S., Bershadsky, A., et al. (2022). Microtubules tune mechanosensitive cell responses. *Nat. Mater.* **21**, 366–377.

Shah, N., Kumar, S., Zaman, N., Pan, C. C., Bloodworth, J. C., Lei, W., Streicher, J. M., Hempel, N., Mythreye, K. and Lee, N. Y. (2018). TAK1 activation of alpha-TAT1 and microtubule hyperacetylation control AKT signaling and cell growth. *Nat. Commun.* **9**,.

Sieber, O. M., Tomlinson, S. R. and Tomlinson, I. P. M. (2005). Tissue, cell and stage specificity of (epi)mutations in cancers. *Nat. Rev. Cancer* **5**, 649–655.

Singh, A., Saha, T., Begemann, I., Ricker, A., Nüsse, H., Thorn-Seshold, O., Klingauf, J., Galic, M. and Matis, M. (2018). Polarized microtubule dynamics directs cell mechanics and coordinates forces during epithelial morphogenesis. *Nat. Cell Biol.* **20**,

1126–1133.

Szafranski, P. and Goode, S. (2004). A Fasciclin 2 morphogenetic switch organizes epithelial cell cluster polarity and motility. *Development* **131**, 2023–2036.

Tepass, U., Theres, C. and Knust, E. (1990). Crumbs encodes an EGF-like protein expressed on apical membranes of Drosophila epithelial cells and required for organization of epithelia. *Cell* **61**, 787–799.

Tian, J., Han, L., Feng, Z., Wang, G., Liu, W., Ma, Y., Yu, Y. and Kong, Z. (2015). Orchestration of microtubules and the actin cytoskeleton in trichome cell shape determination by a plant-unique kinesin. *Elife* **4**, e09351.

Timmons, A. K., Mondragon, A. A., Schenkel, C. E., Yalonetskaya, A., Taylor, J. D., Moynihan, K. E., Etchegaray, J. I., Meehan, T. L. and McCall, K. (2016). Phagocytosis genes nonautonomously promote developmental cell death in the Drosophila ovary. *Proc. Natl. Acad. Sci.* **113**, E1246–E1255.

Tumaneng, K., Schlegelmilch, K., Russell, R. C., Yimlamai, D., Basnet, H., Mahadevan, N., Fitamant, J., Bardeesy, N., Camargo, F. D. and Guan, K. L. (2012). YAP mediates crosstalk between the Hippo and PI(3)K-TOR pathways by suppressing PTEN via miR-29. *Nat. Cell Biol.* **14**, 1322–1329.

Wells, R. E., Barry, J. D., Warrington, S. J., Cuhlmann, S., Evans, P., Huber, W., Strutt, D. and Zeidler, M. P. (2013). Control of tissue morphology by Fasciclin III-mediated intercellular adhesion. *Dev.* **140**, 3858–3868.

Wu, X., Tanwar, P. S. and Raftery, L. A. (2008). Drosophila follicle cells: Morphogenesis in an eggshell. *Semin. Cell Dev. Biol.* **19**, 271–282.

Xiong, F., Ma, W., Hiscock, T. W., Mosaliganti, K. R., Tentner, A. R., Brakke, K. A., Rannou, N., Gelas, A., Souhait, L., Swinburne, I. A., et al. (2014). Interplay of cell shape and division orientation promotes robust morphogenesis of developing epithelia. *Cell* **159**, 415–427.

Xu, Z., Schaedel, L., Portran, D., Aguilar, A., Gaillard, J., Peter Marinkovich, M., Théry, M. and Nachury, M. V. (2017). Microtubules acquire resistance from mechanical breakage through intralumenal acetylation. *Science (80-.).* **356**, 328–332.

Yan, C., Wang, F., Peng, Y., Williams, C. R., Jenkins, B., Wildonger, J., Kim, H. J., Perr, J. B., Vaughan, J. C., Kern, M. E., et al. (2018). Microtubule acetylation is required for mechanosensation in Drosophila. *Cell Rep.* **25**, 1051–1065.

Main Figure Legends

Fig. 1. Microtubule acetylation underpins cell flattening in diverse squamous epithelial cells.

(**A-B**) Cadherin (grey) marks the cell boundaries of the follicle epithelium at various stages of development. The stage 10 egg chamber (A) is marked for anterior squamous follicle epithelium covering the underlying nurse cells, SE(N), and posterior columnar epithelium encapsulating oocyte CE(O). By stage 14 (B), CE(O) stretches to encapsulate the growing oocyte and becomes squamous, denoted as SE(O). Cartoon representation of the top view of stage 10 and stage 14 follicle epithelium (C). Abbreviations: SE (squamous epithelium) CE, (columnar epithelium) N, (nurse cells); O (oocyte).

(**D-H**) Top view of stage 10 (D-E) and stage 14 follicle epithelium (F) immunostained for acetylated tubulin (magenta). Quantification to compare the cell area (G) and acetylated microtubule (acet-MT) fluorescence intensity per unit area (H) for the indicated cell types.

(**I-K**) Top view of pupal (I) and adult MAG (J) stained for cadherin (grey). Cartoon representation (K) to display comparison of MAG organ and cell area between pupal columnar epithelia, CE(MAG), and adult squamous epithelia SE(MAG).

(**L-O**) Top view of columnar, CE(MAG) (L), and squamous, SE(MAG) (M) immunostained for acetylated tubulin (magenta). Quantification to compare the cell area (N) and acet-MT fluorescence intensity per unit area (O) for the indicated cell types.

(P-U) In comparison to control stage 14 squamous follicle epithelium (P-P'), *α-tat* knockdown in SE(O) display reduced cell size (Q-Q', see T for quantification) and wiggly cell boundaries marked cadherin (grey). Likewise, *α-tat* knockdown also reduces MAG cell size compared to the control (R-S'). The cell boundaries are marked with FasIII (grey). Quantification of cell area of follicle, SE(O) (T) and MAG, SE(MAG) (U) in control and *α-tat-IR*.

(**V**) Schema representing the unified principle of microtubule acetylation-dependent cell flattening in both squamous tissue types, MAG and follicle.

Scale bar: (A-B, I-J, R-S) 100 µm, (P-Q) 50 µm, (D-F, L-M, all insets) 10 µm.
Data analysed by unpaired *t*-test: ****p<0.0001 and ***p=0.0005

Fig. 2. Loss of microtubule acetylation inhibits membrane proteins dilution and compromises epithelial flattening.

(**A-C'**) Squamous epithelia of follicle, SE(O) with *α-tat* knockdown show robust cell boundaries (white, grey) as marked by septate junction protein Fasciclin III, Fas III (A-A'), sub-apical cell-cell junction protein Cadherin, Cad (B-B'), and basolateral membrane polarity protein Lethal giant larvae, Lgl (C-C'). In all inverted images (A'-C'), compare the cell boundaries *α-tat* knockdown somatic clones (red*), with surrounding wild-type cells (blue*).

(**D-F**) Quantification of normalised fluorescence intensity of FasIII (D), Cadherin (Cad, E) and Lgl (F) in wild type (WT) and *α-tat* knockdown cells (green nuclei) in follicle SE(O).

(**G-I'**) Somatic clones with *α-tat* knockdown (green) in a 5-day-old SE(MAG) show robust cell boundaries (white, grey) in comparison to wild-type (GFP-negative clones), as marked by FasIII (G-G'), Cad (H-H'), and Lgl (I-I'). In all inverted images (G'-I'), compare the cell boundaries *α-tat* knockdown somatic clones (red*), with surrounding wild type cells (blue*).

(**J-L**) Quantification of normalised fluorescence intensity of FasIII (J), Cadherin (Cad, K) and Lgl (L) in wild type (WT) and *α-tat* knockdown cells (green nuclei) in SE(MAG).

(**M-N**) Somatic clones with *α-tat* knockdown (green) in SE(O) display Rab5 vesicles (green) lodged at the cell periphery (M). Images at higher magnification of another follicle reveal large Rab 5 vesicles lodged at the cell periphery of *α-tat* knockdown (blue) cells (N).

(**O-P**) Somatic clones with *α-tat* knockdown (blue) in SE(O) display Lgl (magenta) colocalized with Rab 5 (green). Inset magnified in adjacent panel (O') to reveal colocalization (white puncta, yellow arrowhead). Quantification of colocalization of Lgl and Rab5 in WT and *α-tat* knockdown cells (P).

(**Q**) Schema to represent microtubule acetylation loss-mediated (blue nuclei) sequestration of membrane proteins (Lgl, magenta) due to defective early endocytosis (Rab5, green).

Scale bar: (A-I', N, O') 10 µm, (M, O) 50 µm.
Data analysed by unpaired *t*-test: ****p<0.0001; ***p=0.0003 (F) and ***p=0.0002 (P)

Fig. 3. Microtubule acetylation regulates actin remodeling during epithelial flattening.
(A-B'') Somatic clones with *α-tat* knockdown (blue) in the SE(O) stained for actin (phalloidin, green/grey), Lgl (magenta), and cofilin (white/grey).

(**C-D**) SE(MAG)-specific expression of Life-act RFP (grey) in the control and *α-tat* knockdown.

(**E**) Cartoon representation showing the significance of actin (green) and acetylated microtubule crosstalk in epithelial flattening. The illustrations are explained in the lower panel.

Scale bar: (A-B'') 10 µm; (C-D) 50 µm.

Fig. 4. Yorkie differentially regulates microtubule acetylation in SEs of MAG and follicle.
(**A-A'**) Somatic clones in SE(O) with *α-tat* knockdown (RFP-negative nuclei) (A-A') display nuclear Yki-GFP (green).

(**B-C**) The adult MAG epithelium of control (B), and *α-tat* loss (C) display nuclear Yki-GFP. Nuclei are marked by TO-PRO (red) and FasIII (white) marks the cell boundaries. Yellow nuclei indicate colocalisation of Yki-GFP with the nucleus.

(**D-K**) In comparison to control SE(O) (D), yki loss in SE of ovarian follicle display a decrease in microtubule acetylation (E, grey). Note that acetylated microtubules only stain the overlying muscle of the egg chamber and not the epithelial cells in SE with yki loss. The adult MAG immunostained for microtubule acetylation (grey) in the control (F) and yki loss (G). Note the increase in acetylation staining in MAG with yki loss. Upregulated TOR signaling in adult ovarian follicles (*c204>myr-Akt*) displays enhanced levels of microtubule

acetylation (red arrowheads, H), compared to acetylated tubulin in downregulated TOR signaling (*c204>Akt-IR*) (I). Adult MAGs with TOR modulation (*ov>myr-Akt* (J) and *ov>Akt-IR* (K)) immunostained for acetylated microtubule.

(**L-N**) In comparison to the control (L), *α-tat* loss (M) displays upregulated levels of pS6K (magenta). Quantification to compare fluorescence intensity of pS6K in control and SE(O) with *α-tat* loss.

(**O-Q**) Comparison of pS6K expression in adult MAGs of control (O) and *α-tat* knockdown (ov>*α-tat-IR*, P), and its quantification (Q).

Scale bar: (A-A', D-P) 50 µm, (B-C) 10 µm.
Data analysed by unpaired *t*-test: ****p<0.0001

Fig. 5. Microtubule hyperacetylation induces MAG-SCC.

(**A-C**) MAG stained for actin (phalloidin, green) to indicate organ size in control (A), HDAC6 knockdown (B), and quantified (C).

(**D-D'**) Prolonged knockdown of HDAC6 (20D) (somatic clones, green) results in disruption of MAG cell architecture (FasIII, grey/white).

(**E-E''**) HDAC6 knockdown displays active Yki signaling, as indicated by Diap1-lacZ (green) expression in the nuclei (red).

(**F-H**) In comparison to the control (F), knockdown of HDAC6 (G) display elevated levels of pS6K, also quantified (H).

(**I-K''**) α-tubulin (green) and acetylated tubulin (acet-MT, magenta) immunostaining of control (I-I''), yki loss (J-J'') and *ov>α-tat-IR, yki-IR* MAGs (K-K''). Note the increased fluorescence intensity of acetylated and alpha tubulin in yki loss-mediated MAG-SCC model.

(L-N) MAG cell boundaries immunostained for FasIII (grey) in control (L), yki loss (M), and *ov>α-tat-IR, yki-IR* (N).

(**O-P**) Quantification of the cell area for the indicated genotypes in MAG (O). Kaplan-Mier survival plot of adult flies of indicated genotypes in MAG (P).

Scale bar: (A-D) 100 µm, (I-N) 10 µm, (E-G) 50 µm.

Data analysed by unpaired *t*-test: ****$p<0.0001$ and ***$p=0.0008$

Figure 1

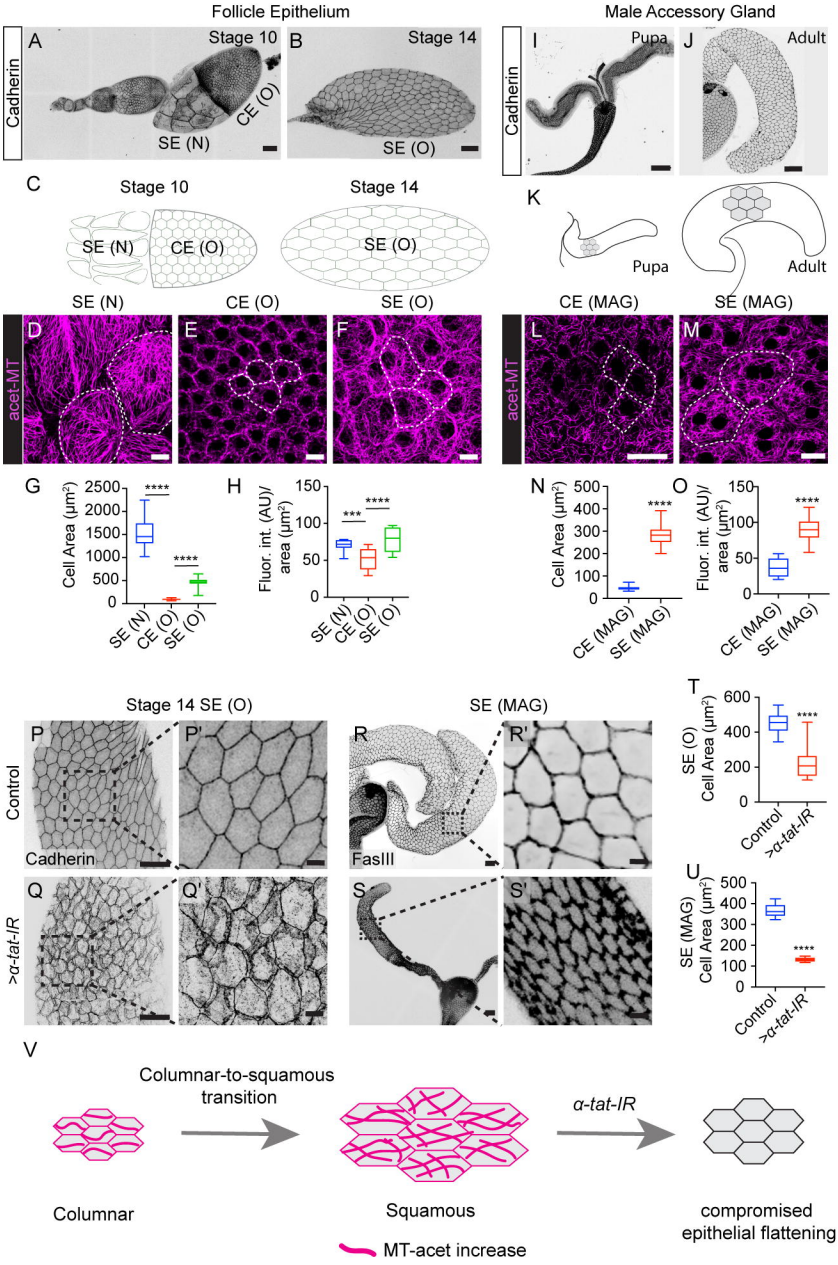
Follicle Epithelium
Male Accessory Gland
A
Stage 10
B
Stage 14
Cadherin
CE (O)
SE (N)
SE (O)
I
Pupa
J
Adult
C
Stage 10
Stage 14
SE (N)
CE (O)
SE (O)
K
Pupa
Adult
SE (N)
CE (O)
SE (O)
CE (MAG)
SE (MAG)
D
E
F
L
M
acet-MT
G
Cell Area (μm²)
****
****
SE (N)
CE (O)
SE (O)
H
Fluor. int. (AU)/ area (μm²)
***
****
N
Cell Area (μm²)
****
CE (MAG)
SE (MAG)
O
Fluor. int. (AU)/ area (μm²)
****
Stage 14 SE (O)
SE (MAG)
Control
>α-tat-IR
P
P'
R
R'
Cadherin
FasIII
Q
Q'
S
S'
T
SE (O) Cell Area (μm²)
****
Control
>α-tat-IR
U
SE (MAG) Cell Area (μm²)
****
V
Columnar-to-squamous transition
α-tat-IR
Columnar
Squamous
compromised epithelial flattening
MT-acet increase

Figure 2

hs-flp, act>α-tat-IR

SE(O)

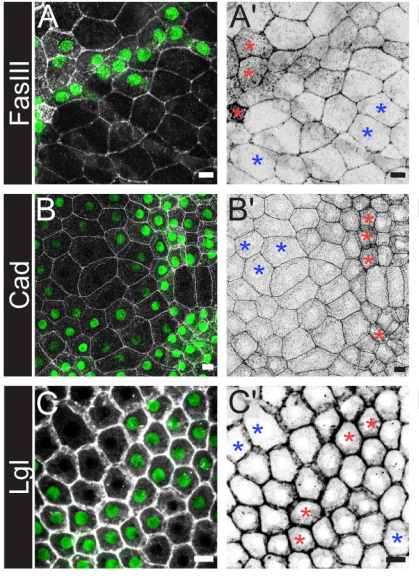

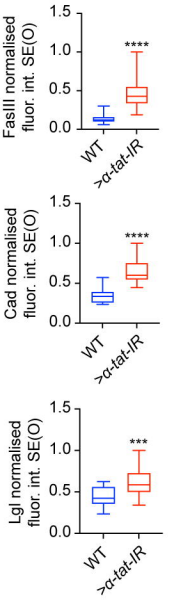

SE(MAG)

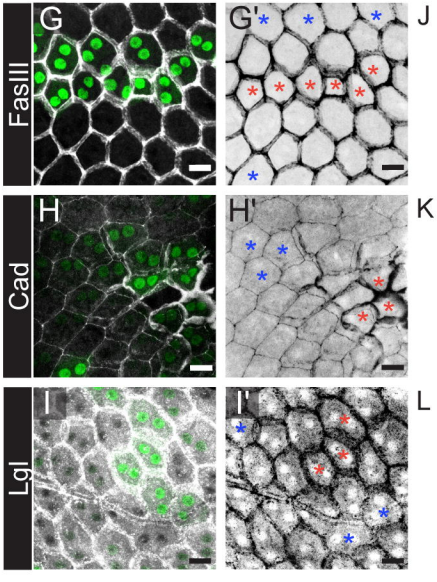

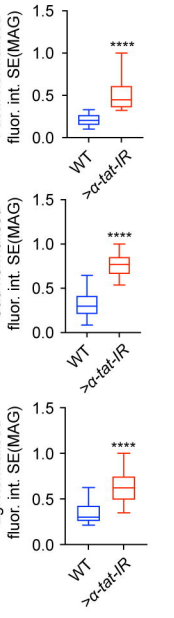

hs-flp, act>α-tat-IR

SE(O)

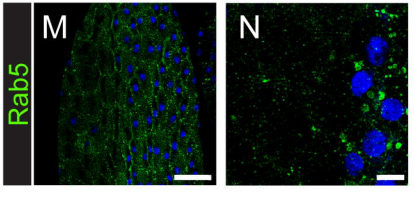

hs-flp, act>α-tat-IR

SE(O)

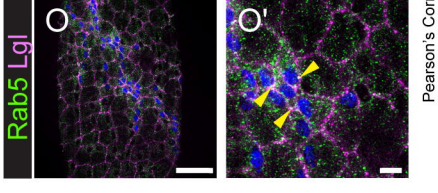

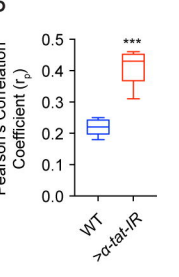

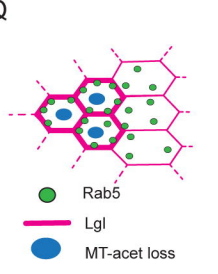

Figure 3

hs-flp, act>α-tat-IR

Actin Lgl | Actin | Lgl

SE(O)

A | A' | A''

hs-flp, act>α-tat-IR

Cofilin GFP | Cofilin | GFP

SE(O)

B | B' | B''

Control | *ov>α-tat-IR*

Life-Actin

SE(MAG)

C | D

E

Control

MT-acet loss

Memb. Proteins

Actin

Cofilin

Figure 4

Stage 14 SE (O)

hs-flp, act>α-tat-IR (RFP-)

yki-GFP RFP

A

A'

SE (MAG)

Control

>α-tat-IR

yki-GFP Nuclei FasIII

B

C

acet-MT

Control

>yki-IR

D

E

>myr-Akt

>Akt-IR

H

I

acet-MT

Control

>yki-IR

F

G

>myr-Akt

>Akt-IR

J

K

pS6K

Control

>α-tat-IR

L

M

pS6K

Control

>α-tat-IR

O

P

N

pS6K normalised fluor. int. SE(O)

1.5

1.0

0.5

0.0

****

Control

>α-tat-IR

Q

pS6K normalised fluor. int. SE(MAG)

1.5

1.0

0.5

0.0

****

Control

>α-tat-IR

Figure 5

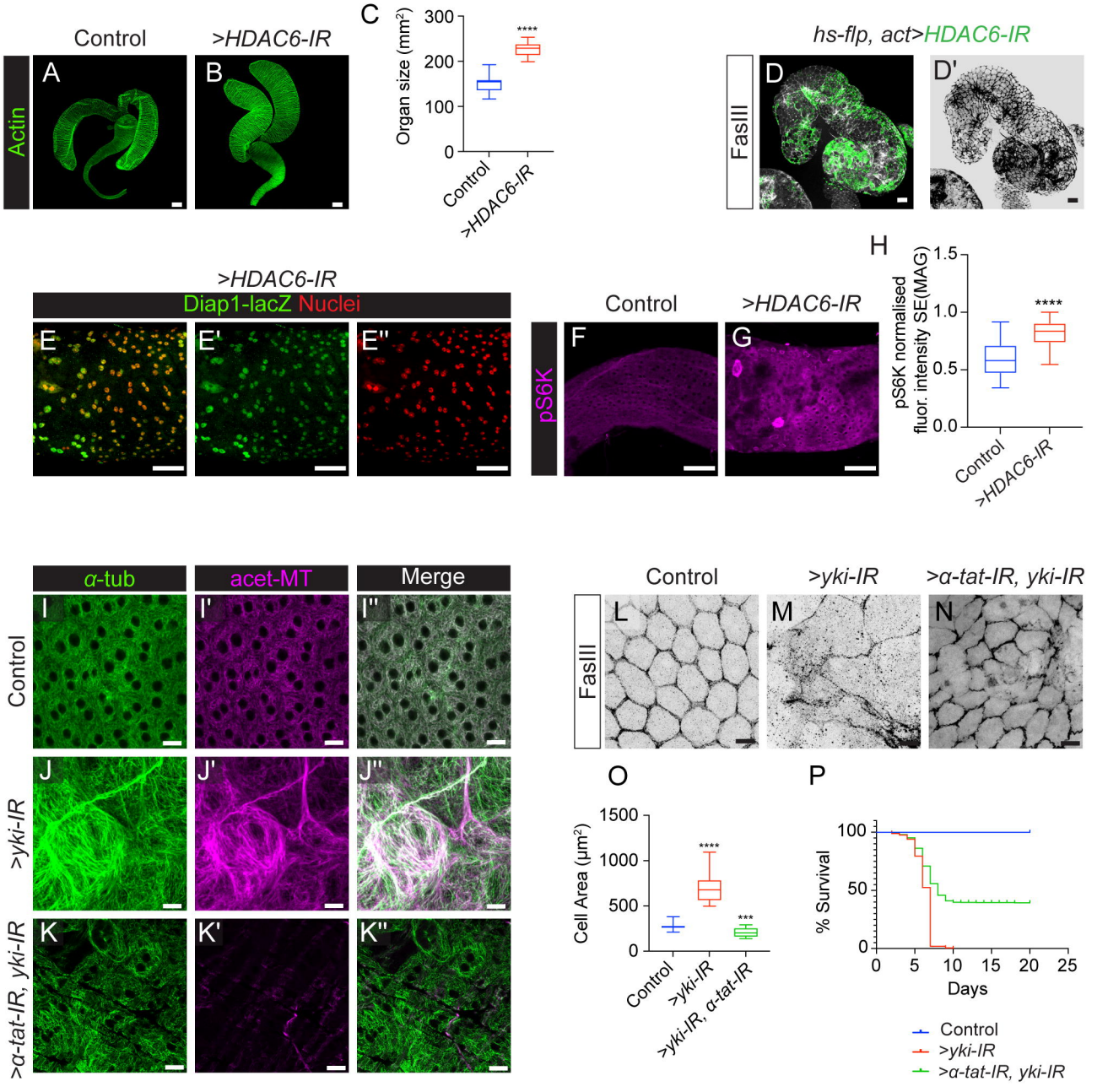
Control
>HDAC6-IR
Actin
A
B
C
Organ size (mm²)
300
200
100
0
****
Control
>HDAC6-IR
hs-flp, act>HDAC6-IR
FasIII
D
D'
>HDAC6-IR
Diap1-lacZ Nuclei
E
E'
E''
Control
>HDAC6-IR
pS6K
F
G
H
pS6K normalised fluor. intensity SE(MAG)
1.5
1.0
0.5
0.0
****
Control
>HDAC6-IR
α-tub
acet-MT
Merge
Control
>yki-IR
>α-tat-IR, yki-IR
I
I'
I''
J
J'
J''
K
K'
K''
Control
>yki-IR
>α-tat-IR, yki-IR
FasIII
L
M
N
O
Cell Area (μm²)
1500
1000
500
0
****
***
Control
>yki-IR
>yki-IR, α-tat-IR
P
% Survival
100
50
0
0
5
10
15
20
25
Days
Control
>yki-IR
>α-tat-IR, yki-IR